Spatial variability in river bed porosity determined by nuclear density gauging: A case study from a French gravel-bed river

MINA TABESH*,† ⓘ, STEFAN VOLLMER†, HOLGER SCHÜTTRUMPF* and ROY M. FRINGS‡

*Institute of Hydraulic Engineering and Water Resources Management, RWTH Aachen University, Mies-van-der-Rohe-Straße 17, 52074, Aachen, Germany (E-mail: tabesh@iww.rwth-aachen.de)
†Department of Fluvial Morphology, Sediment Dynamics and Management, Federal Institute of Hydrology, Am Mainzer Tor 1, 56068, Koblenz, Germany
‡Rijkswaterstaat Zuid-Nederland, Ministry of Infrastructure and Water Management, Avenue Ceramique 125, 6221 KV, Maastricht, Netherlands

ABSTRACT

Porosity is one of the key properties of fluvial sediments. It is defined as the ratio of pore volume to total volume. In river science, porosity is often assumed to be spatially constant, which might be a gross simplification of reality. Ignoring the spatial variations in porosity can cause errors in morphological, ecological, hydrological, hydrogeological and sedimentological applications. Although detailed information about spatial porosity variations can be obtained from porosity measurements at field sites, such information has never been collected where these variations might be important. In this study, field porosity measurements were carried out to quantify the magnitude of the spatial porosity variation for four different sedimentological environments of a braided river: a confluence, a tributary delta, a braid bar and a secondary channel. A nuclear density gauge was used for the measurement of porosity. The nuclear density gauge proved to be a time-saving and labour-saving technique that produces accurate porosity values with a root mean square error of 0.03. The four sedimentological environments showed significant differences in porosity, with mean porosity being lower for confluence and bar than for delta and secondary channel. Semi-variogram analysis showed the absence of any spatial correlation in porosity for distances beyond 4 m. This shows that distance cannot be used as a parameter for porosity extrapolation in a fluvial system unless the extrapolation distance is less than 4 m. At least eight measurements of porosity are required to obtain a reliable estimate of mean porosity in a sedimentary environment, i.e. with uncertainty <0.03. Although grain size characteristics were found to have a significant impact on porosity, the relationships between these parameters and porosity were not very strong in this study. The unique porosity dataset, presented in this article, provides a valuable source of information for researchers and river managers.

Keywords Fluvial sand-gravel mixtures, *in situ* measurement, nuclear density gauge, porosity, semi-variogram analysis, spatial variation.

INTRODUCTION

Total sediment porosity [hereinafter called 'porosity (*n*)'], defined as the ratio of pore volume to total volume, is one of the key structural properties of a river bed. River bed porosity strongly affects river morphology through its control on the rate of bed level changes (it is an important parameter in the Exner equation), interstitial flow processes, initiation of sediment motion, energy dissipation and gravel–sand transitions (e.g. Chwang & Chan, 1998; Wilcock, 1998; Ting *et al.*, 2004; Vollmer & Kleinhans, 2007; Frings *et al.*, 2008; Frings, 2011; Abderrezzak *et al.*, 2016; Miwa & Parker, 2017; Mulatu *et al.*, 2018; Bui *et al.*, 2019). Furthermore, reconstruction of sediment fluxes from measured morphological changes, for example, by dune tracking or sediment budgeting (Frings *et al.*, 2014; Church & Ferguson, 2015), also requires information about porosity. Porosity furthermore controls the ecological suitability of a river bed as a habitat for aquatic organisms (e.g. Boulton *et al.*, 1998; Argent & Flebbe, 1999; Vollmer *et al.*, 2002; Wooster *et al.*, 2008; Noack, 2012). Moreover, it determines the exploitable volume of oil, gas and groundwater contained in the pores of geological deposits (e.g. Athy, 1930), and affects the hydraulic conductivity of sediment mixtures (Koltermann & Gorelick, 1995; Morin, 2006; Zhang *et al.*, 2011). Finally, porosity has an influence on other structural properties such as permeability (Hatch *et al.*, 2010), and thus detailed information about porosity variations could help to better understand permeability changes occurred within porous river beds, which, for instance, enhances models that represent the hierarchical stratal architecture of fluvial deposits (Ramanathan *et al.*, 2010).

Until now, little is known about the magnitude of spatial variations in porosity in fluvial sand–gravel systems. Porosity of sand–gravel mixtures is known to vary between 0.1 and 0.5 (e.g. Selby, 1993; Domenico & Schwartz, 1998) but, for most practical applications in river science, porosity is often simply assumed to be spatially constant. For example, in the numerical model developed to study downstream fining processes in sand-bed rivers, Frings *et al.* (2011a) assumed a constant porosity of 0.34. With the assumption of a constant porosity of 0.3, Cui (2007) developed a numerical model to study the dynamics of grain size distributions on the channel bed surface.

Previous investigations have revealed the presence of spatial variations in porosity in the Rhine River (Frings *et al.*, 2008, 2011b, 2012; Frings, 2011) at length scales from 1 to 1000 km. However, little is known about porosity variations at smaller length scales (1–100 m). Such small-scale porosity variations are important though, because a failure to account for them can cause bias in morphological, ecological, hydrological, hydrogeological and sedimentological studies. Furthermore, knowledge about the variability in porosity is needed to determine the number of measurements required to obtain a good estimate of the mean porosity at a study site.

Porosity variations at small length scales are likely to occur in rivers, because grain size, known to be one of the major porosity controlling factors in rivers (Carling & Reader, 1982; Wu & Wang, 2006; Wooster *et al.*, 2008; Frings *et al.*, 2011a; Desmond & Weeks, 2014), also varies strongly over these distances due to sorting processes such as dune sorting, bend sorting, patchiness, armouring and downstream fining (Church *et al.*, 1991; Paola & Seal, 1995; Seal & Paola, 1995; Lisle & Hilton, 1999; Kleinhans, 2001, 2005; Kleinhans *et al.*, 2002; Ryan *et al.*, 2002; Blom, 2003; Hassan *et al.*, 2006; Clayton & Pitlick, 2007).

The reason that knowledge about spatial variation of river bed porosity is limited, is the difficulty of porosity measurements in sand–gravel mixtures. Porosity measurement techniques for such mixtures can be divided into direct and indirect methods. Characteristic for direct methods (e.g. Frings *et al.*, 2011a, 2012; Seitz *et al.*, 2018) is that both the solid fraction volume (V_s) and the total volume (V_t) of a sediment sample are measured directly, so that porosity (*n*) can be calculated as:

$$n = 1 - \frac{V_s}{V_t} \qquad (1)$$

Indirect techniques, such as nuclear density gauging (NDG) relate porosity to other sediment properties (for example, mineral density, pore water content or grain size characteristics), which can be measured more easily. Although indirect methods allow for an easy and quick porosity assessment, they always require calibration, which is not the case for the more time-intensive and labour-intensive direct methods.

This study investigated the spatial variability of porosity in various sedimentological environments of a braided river: a confluence, a

tributary delta, a braid bar and a secondary channel. For this purpose, an extensive porosity dataset was obtained using NDG, a technique which has not been yet used for porosity measurement in rivers.

Our research aimed at answering the following questions:

1 Is nuclear density gauging (NDG) a suitable technique for measuring porosity in sand–gravel bed rivers?

2 Do the various sedimentological environments in braided rivers show different porosity?

3 Is porosity variation within sedimentological environments essentially random, or is there a spatial correlation, causing nearby locations to have similar porosity?

4 How many porosity measurements are required to obtain a good estimate of the mean porosity in a field site?

5 Can porosity variations be explained by the variations of grain size characteristics?

STUDY AREA

The study was carried out in the south-eastern part of France in the region of Rhône–Alpes (Fig. 1). The Mediterranean climate with dry summers and elongated low-flow periods is favourable for porosity measurements, because they cause the exposure of extensive, natural sediment deposits with different lithologies, grain sizes and grain shapes. In this region, two different rivers were selected for porosity measurements: the Bès River and the Galabre River. The Bès River is a braided gravel-bed river confluencing with the Bléone River near the town of Digne-les-Bains. It has a length of about 34 km and a drainage basin of 233 km^2 (Navratil et al., 2012). The elevation of its catchment ranges from 640 to 2700 m above sea level. The average width of the active braid plain is approximately 60 m, varying from 50 to 180 m. The mean annual precipitation is 930 mm. The Bès River has a perennial flow regime. Flow data have been recorded at the Pérouré gauging station since 1963, showing the river's mean flow discharge to be about 2.83 m^3 s^{-1}. The peak discharges of the two-year, five-year and ten-year return periods are 58 m^3 s^{-1}, 100 m^3 s^{-1} and 130 m^3 s^{-1}, respectively (Navratil et al., 2010). Forest is by far the main land use in the catchment covering 70% of the total surface. The lithology of the Bès River basin comprises a great proportion of limestone and marl, followed by a small proportion of gypsum and sandstone (Navratil et al., 2010).

The Galabre River is a headwater tributary of the Bès River. This river has a drainage basin of 35 km^2 and a length of 7 km. Its braid plain is approximately 10 m wide. The mean annual precipitation is 1000 mm. The Galabre is a perennial river with an average discharge of
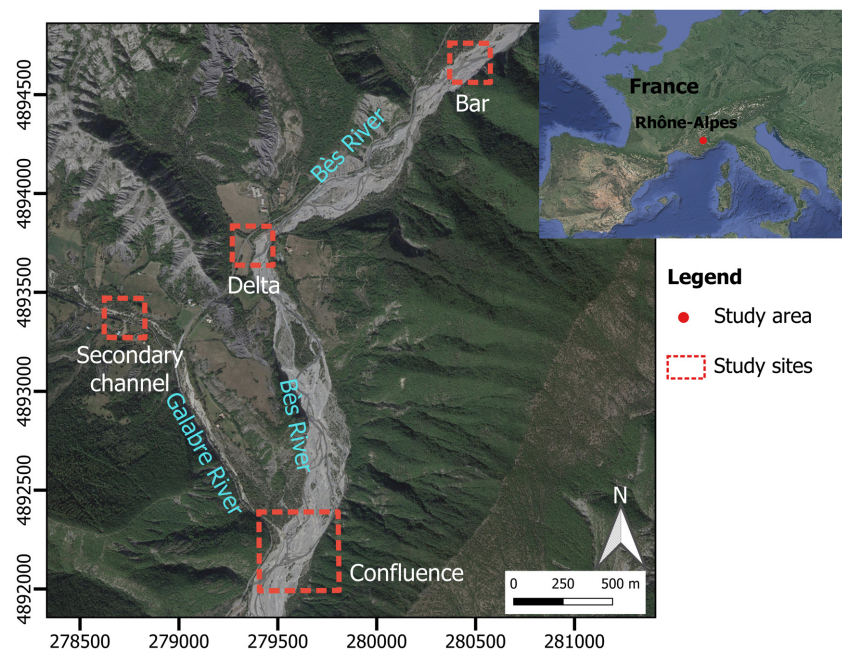
Fig. 1. The study area located in south-eastern France: three study sites with different sedimentological facies (a braid bar, a tributary delta and a confluence) along the Bès River and one (a secondary channel) along the Galabre River.

0.1 m^3 s^{-1} and a low flow discharge of 0.02 m^3 s^{-1} during summer. The maximum discharge ever recorded is 34 m^3 s^{-1} (Navratil *et al.*, 2012). The catchment of the Galabre is mostly covered with forest (52%) and scrubland (30%). The lithology of this catchment is composed of various sedimentary rocks; mainly limestones, marls and marly limestones, gypsum, molasses and Quaternary deposits (Esteves *et al.*, 2019). In this river, the bed sediments mainly consist of gravel, cobbles and boulders.

To measure porosity, four sites were selected (Fig. 1). The first three sites are located along the Bès River representing different sedimentological environments: a braid bar, a tributary delta and a confluence. The fourth site, a secondary channel, is located along the Galabre River. Detailed morphological maps of each site, constructed in the field, and then digitized in QGIS software, are shown in Fig. 2.

The first site, the braid bar, was in the centre of the braid plain located in the upstream reach of the Bès River (latitude: 44°10'20''N, longitude: 06°15'14''E). This bar had a length of 60 m and a maximum width of 15 m. Its surface was composed of sand, gravel and cobbles. The braid bar consisted of a main bar with an extension to the right side (Fig. 2A). The main bar was covered by several small dry channels discharging to the left side (relative to the downstream direction) of the bar. The braid channel at the orographic left side of the bar had a lower water level than the one on the right side relative to the downstream direction. The second site, the tributary delta, was located 1.5 km downstream from the first site (latitude: 44°09'48''N, longitude: 06°14'26''E) where the torrent de St. Vincent, an ephemeral stream, entered the Bès channel deposit and formed a small delta (Fig. 2B). At the time of measurement, the delta was dry. The length of the site was 62 m and its maximum width 14 m. The delta surface was approximately 1.5 m lower than the surrounding Bès terrace. The sediments consisted of black marls. Sedimentologically, the delta was homogenous with no clear grain size trends. The third site (latitude: 44°08'58''N, longitude: 06°14'36''E) was the confluence of the Bès River and the Galabre River (Fig. 2D). The width of the braid plain was approximately 180 m. This study site had a length of 190 m and extended over the full width of the braid plain. The confluence site incorporated both bars and channels. Approximate bar lengths are between 28 m and 100 m and widths between 6 m and 35 m. The width

of the braid channels was approximately 10 m. Vegetated patches were scattered between the dry river channels. The sediments consisted of cobbles, gravel and sand. The fourth study site, the secondary channel, was located in the Galabre River (latitude: 44°09'37''N, longitude: 06°13'59''E) (Fig. 2C). This site had a length of 62 m and a maximum width of 6 m. Its sediment surface was dominated by sand and gravel.

METHODS

Nuclear density gauging

To quantify spatial variations in porosity, extensive porosity data are needed. In the past, a few studies have been done that provided detailed information on the spatial variability in porosity in sand–gravel bed rivers. Most of these studies aimed at identifying the relationship between porosity and its controlling factors (e.g. Carling & Reader, 1982) with no focus on the spatial variability of porosity. Only Frings *et al.* (2011a, 2012), who worked on the Rhine River, provided information on the spatial variability in porosity. However, they focused on porosity trends on larger scales (1–1000 km) and did not provide information about the magnitude of spatial porosity variations at the local scale.

Therefore, this study carried out new porosity measurements. These measurements were made by NDG, a technique normally used for sand and asphalt compaction tests in civil construction. Nuclear density gauges (NDGs) measure the total wet density and the water content of a sediment surface, from which porosity (n) can be calculated if the mineral density is known as:

$$n = 1 - \frac{\rho_t}{\left(1 + \frac{\eta}{100}\right)\rho_s} \quad (2)$$

where ρ_t is the wet mass per unit volume (kg m^{-3}), η is the mass of the pore water per mass of solid fraction (%), and ρ_s is the mineral density which is the mass per unit volume of the solid fraction (kg m^{-3}).

For measurement of the total wet density, the NDG contains a Caesium-137 source, emitting gamma radiation. Detector tubes at the edge of the gauge count the number of gamma particles that pass through the sediment (Fig. 3A). The denser the sediment, the lower the number of gamma particles that reaches the detector tubes. For measurement of the water content, the NDG
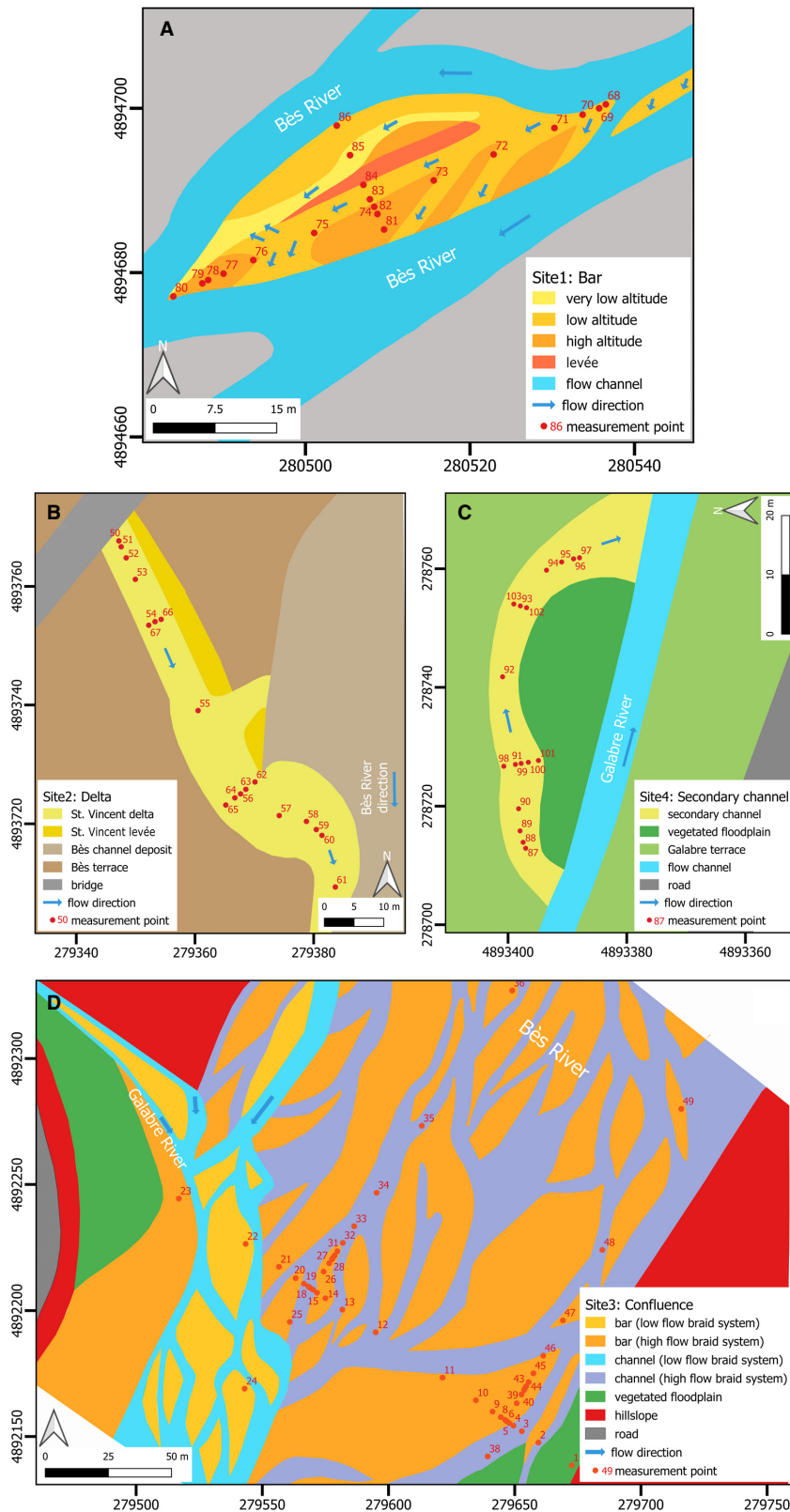
Fig. 2. The morphology of the measurement sites: (A) bar; (B) delta; (D) confluence along the Bès River; and (C) secondary channel along the Galabre River. Coordinate system WGS 84/UTM zone 32N (EPSG:32632).
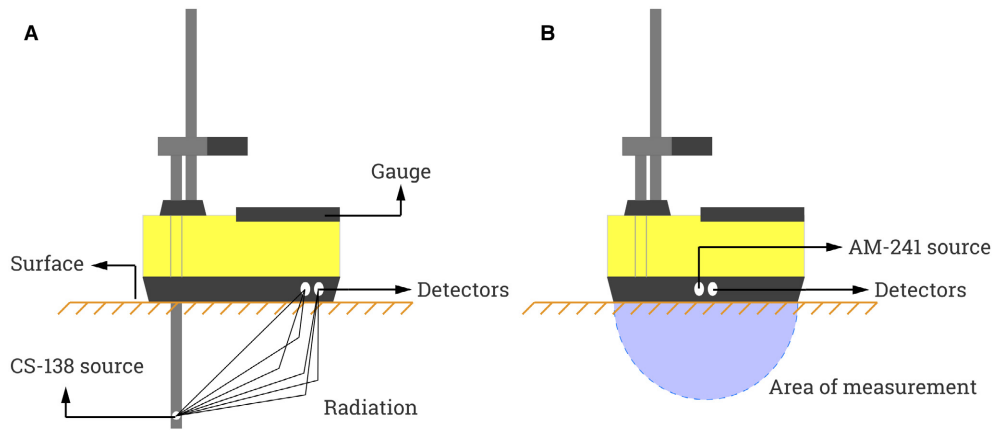
Fig. 3. Nuclear density gauge (NDG): (A) direct transmission total wet density measurement; (B) backscatter water content measurement.

contains a source of Americium-241, emitting high energy neutron particles. These neutrons are scattered back and slowed down by the sediment containing hydrogen below the gauge. Detectors count the number of slow neutrons returning to the gauge. Because especially materials containing hydrogen slow down the neutrons, higher counts indicate a higher moisture content (Fig. 3B).

A Humboldt 5001EZ type NDG was used, in the so-called direct transmission mode, to measure porosity at the four sites in Bès River and Galabre River described above. Because NDGs do not work under water, the field campaign was conducted during a low-flow period in summer (July 2019). At all four sites, the sample positions were distributed in the cross-sectional and longitudinal directions (Table 1).

At the start of each field day, a reference measurement on a rectangular block of plastic

material was made with the NDG to ensure that it was operating correctly, as prescribed by the manufacturer. Before starting an NDG measurement in the field, the armour layer with a thickness of about two grains was carefully removed until the homogeneous gravel–sand deposits of interest became exposed. The sediment surface was then levelled to provide a tight contact between NDG and sediment. This reduced the chance that protruding stones impact the reading with the device. After installing the gauge, the rod containing the Caesium-137 source was extended through the base of the gauge into a predrilled hole and positioned at a depth of 0.1 m. At each location, three successive measurements were carried out without displacing the NDG and a time interval of 1 min was used as counting period. Using the NDG a total of 103 measurements was made. At two points (22 and 93), no NDG porosity value could be obtained

Table 1. Sample position distribution in cross-sectional and longitudinal profile at four measurement sites: η, water content; ρ_t, total wet density; ρ_s, mineral density; V_s, solid fraction volume; V_t, total volume of a sediment sample.

Site	Name	River	Number of cross-sectional profiles	Number of longitudinal profiles	Number of measurements *in situ*			Number of measurements *ex situ*			
					η	ρ_t	V_t	η	ρ_s	V_s	V_t
Site 1	Bar	Bès River	1	1	19	19	3	4	19	19	19
Site 2	Delta	Bès River	2	1	18	18	1	5	5	5	5
Site 3	Confluence	Bès River	1	2	49	49	3	10	14	14	14
Site 4	Secondary channel	Galabre River	2	1	17	17	3	4	17	17	17
Sum					103	103	10	23	55	55	55

due to the direct contact of the NDG with water or with a large stone. Thus, 101 porosity data points were obtained.

Mineral density determination

At 55 of the 101 measurement points, immediately after the NDG measurement, a sediment sample was taken for subsequent laboratory analysis of mineral density (ρ_s). The samples had an average size of about 13 kg (about 7 l) and were obtained from a maximum depth of 10 cm. The samples were sealed in the field, put into boxes and transported into the laboratory, where they were dried for 48 h. Because the sediments contained a small portion of gypsum (a mineral containing waters of crystallization), the oven temperature was set to 80°C (Sadeghiamirshahidi & Vitton, 2019) instead of 105°C. Subsequently, the sediment was put into a cylinder containing a known volume of water to measure the mineral density (ρ_s), using the water displacement method (WDM; Bear, 1972).

Water content correction

At 23 locations, an additional sediment sample was taken from a maximum depth of 10 cm. These samples were sealed and transported into the laboratory where they were weighed, dried and weighed again to determine the water content. These water contents (η_{lab}) were then compared to the water contents measured by the NDG in the field (η_{NDG}; Fig. 4). Although the RMSE (root mean square error) was relatively small (1.7%), the NDG appeared to slightly overestimate the water content, probably because of the presence of waters of crystallization in the crystal lattices of gypsum particles. The relationship between η_{lab} and η_{NDG} ($r^2 = 0.91$), valid for $1.84\% < \eta_{NDG} < 12\%$, was used to correct the NDG-values in the following way:

$$\eta = \max\{0, 1.12\,\eta_{NDG} - 2.06\} \qquad (3)$$

The corrected water contents (Eq. 3) and mineral density values were then used to calculate porosity from Eq. 2.

Semi-variogram analysis

To quantify the spatial variability of porosity, semi-variogram analysis was applied (Matheron, 1963; Cressie & Hawkins, 1980; Cressie, 1985; Deutsch & Journel, 1992; Christakos, 1992),
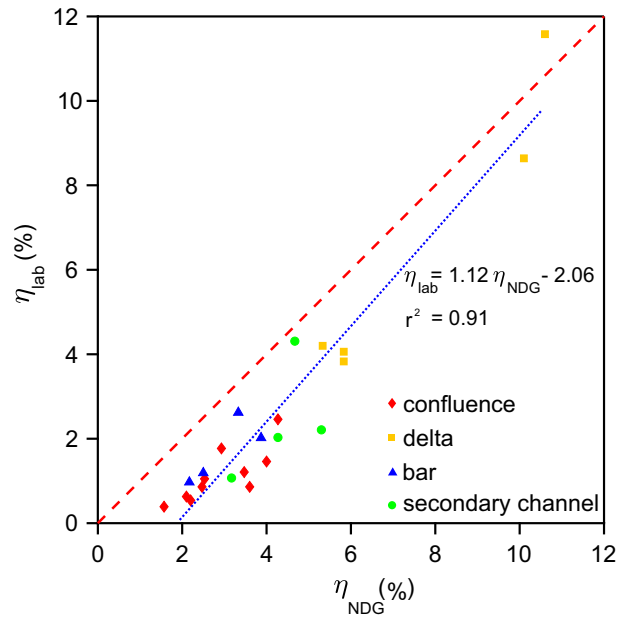
Fig. 4. Water content measured in the laboratory (η_{lab}) versus water content measured in the field (η_{NDG}) for the four measurement sites (coloured dots). Blue dotted line represents regression line (as given by the equation) and red dashed line represents 1 : 1 line.

using the geostatistical methods implemented in the 'gstat' library (Pebesma, 2004).

Experimental semi-variograms were calculated using the following expression:

$$\gamma(h) = \frac{1}{2N(h)} \sum_{i=1}^{N(h)} \{n(x_i + h) - n(x_i)\}^2 \qquad (4)$$

where $n(x_i)$ is the measured porosity value at location x_i and $N(h)$ are the pairs of the measurements that are separated by lag h (the separation between two points). In other words, the semi-variance ($\gamma(h)$) is half of the square of the difference between two values separated by lag h. The semi-variance as a measure of the dissimilarity often increases with increasing lag distance until it levels off to the value denoted as sill. The sill is roughly equivalent to the sample data variance (Gringarten & Deutsch, 2001).

Both isotropic and anisotropic semi-variogram analysis were tried and the isotropic variogram was found to perform better, because of the larger number of measurement points available for bin averaging. Therefore, point pairs were grouped on the basis of distance, not direction.

As shown in Fig. 2, the samples were distributed unevenly over the field sites to maximize the range of the lag interval between samples at each site. As a result, a uniform bin size would either sacrifice the resolution at small lags or under-sample at large lags. Following the methodology developed by Goff *et al.* (2002), bin sizes were chosen dynamically under the criterion that each bin has approximately equal numbers of point pairs. The semi-variogram was computed based on all of the samples from all four sites. The normality requirement was examined by inspecting the histogram of the entire data, showing that the data distribution did not deviate from normality.

Cross-validation of porosity

The porosity data were validated by comparing the porosity values measured with the NDG to porosity values obtained independently with other techniques. This cross-validation procedure consisted of three phases. Firstly, before using the NDG in the field, the device was employed on natural sediments with known total wet density and water content. For this purpose, two boxes ($600 \times 400 \times 320$ mm) were filled with a known amount of an oven-dried sand–gravel mixture. Box 1 contained sediment with $D_{10} = 9.8$ mm, $D_{50} = 21.4$ mm, $D_{90} = 40$ mm and $\sigma_g = 1.74$, and box 2 sediment with $D_{10} = 0.4$ mm, $D_{50} = 11.2$ mm, $D_{90} = 27.5$ mm and $\sigma_g = 4.62$ (see Eq. 7 for a definition of σ_g). Each box was carefully shaken by hand to get a dense packing structure. From the box dimensions and the sediment surface level inside the box, the total volume of the sediment was obtained. Division of the sediment mass by this total volume gave the density of the prototype sediments, which then was used to calculate porosity from Eq. 2 (with $\eta = 0$). Two points on the sediment surface of each box were chosen for the NDG measurement. For each point, the NDG was applied in direct transmission and backscatter mode, with a time interval of 1 min as counting period. Each measurement was done three times without displacing the NDG. Then, 2000 ml of water was added to one of the boxes and the sediment was fully mixed again, levelled and the whole measurement process was repeated. Finally, the resulting NDG–porosity values were compared with the porosity of the prototype sediments.

Secondly, the porosity values measured with the NDG were compared with porosity values measured with the water displacement method (WDM) (Bear, 1972). This was done for 53 of the 55 samples that were taken to the laboratory for the mineral density measurement. For the two remaining samples (samples 11 and 102), a WDM measurement appeared to be impossible because of the presence of large boulders in the sample.

Thirdly, the porosity values measured with the NDG were compared with porosity values measured with yet another technique, namely the photogrammetry method presented by Tabesh *et al.* (2019). This was done for 10 of the 103 NDG positions. At each position, an area of approximately 1×1 m^2 of the bed surface was photographed after the NDG measurement. About 25 oblique pictures were taken from different perspectives with an image overlap of $\geq 80\%$ to ensure adequate image coverage. Afterwards, a pit (approximately $30 \times 30 \times 10$ cm^3) was excavated and the sediment was removed and stored in boxes. After sampling, a new set of images was made using the same procedure covering the excavated surface. Afterwards, the photographs were analyzed using the photogrammetric technique Structure-from-Motion with Multi View Stereo (SfM-MVS; Westoby *et al.*, 2012) implemented in PhotoScan software (1.4.0, Agisoft). In this way, three-dimensional point clouds and DEMs (digital elevation models) of the sediment surfaces before and after excavation were constructed. The difference between the two DEMs provided the total volume of the sediment sample (Tabesh *et al.*, 2019). This total volume was then combined with the measured solid fraction volume to calculate porosity. Two of the photogrammetrically determined porosity values had to be rejected because of problems during total volume measurement in the field.

Finally, the NDG porosity dataset was checked for outliers having porosity values that were atypically high or atypically low. Such outliers are not erroneous, yet fundamentally different from the other porosity data points. Data points were considered to be outliers if they were situated more than three times the interquartile range (IQR) above the upper quartile or three times the IQR below the lower quartile in the boxplot (Fig. 5).

Uncertainty due to water content

The uncertainty in porosity that arises from uncertainties in the water-content correction was also quantified (Eq. 3). The absolute uncertainty of the water contents is equal to the
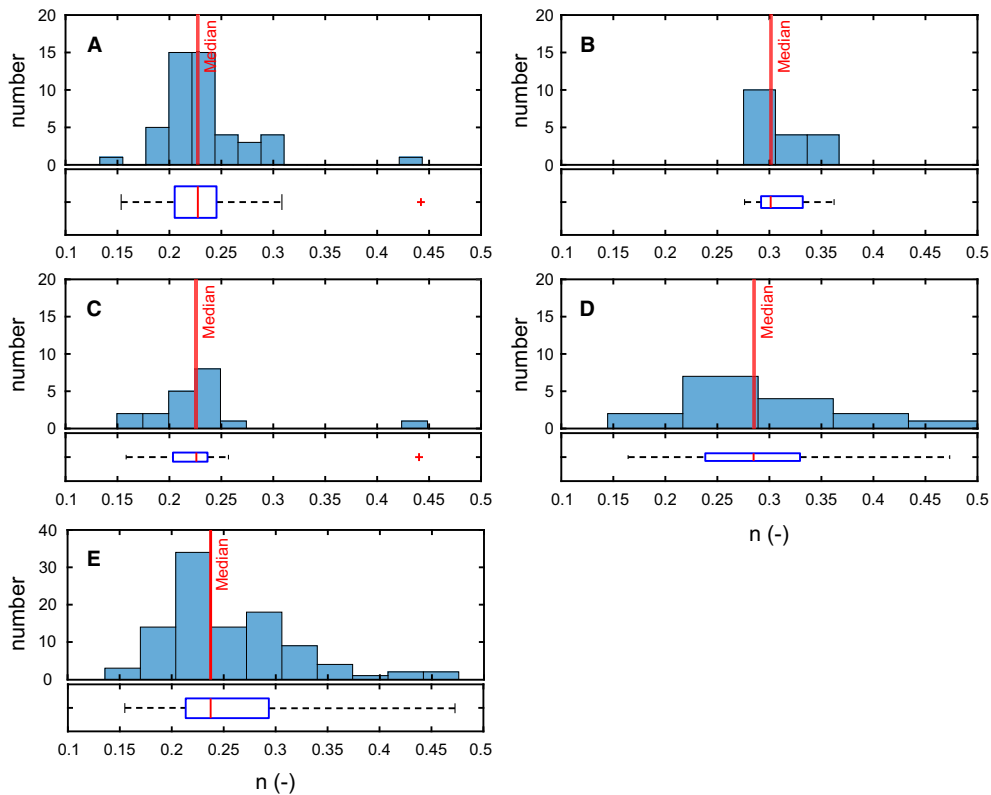
Fig. 5. Histogram and boxplot of nuclear density gauging (NDG) porosity dataset in: (A) confluence; (B) delta; (C) bar; (D) secondary channel; and (E) entire porosity dataset. Bin-widths of histograms are based on interquartile range (IQR) and the number of sampling points at each site (following Freeman–Diaconis rule). Boxplots represent the minimum, first, second (median) and third quartile, and maximum of the porosity at each site. Outliers are shown with red plus sign.

RMSE of the residuals between the water contents measured in the laboratory and the corresponding values calculated using Eq. 3. In our case, it equals 0.77%. The resulting uncertainty in porosity was calculated using an error propagation rule as:

$$\delta n = \left| \frac{\mathrm{d}n}{\mathrm{d}\eta} \right| \delta\eta \tag{5}$$

where δn and $\delta\eta$ are the absolute uncertainty in porosity and water content, respectively, and $\frac{\mathrm{d}n}{\mathrm{d}\eta}$ is the derivative of n (calculated using Eq. 2) with respect to η. In this way, the absolute uncertainty in porosity was found to be ±0.005, resulting in a relative uncertainty of porosity of less than 2.2%.

Grain size analysis

One of the most important factors affecting porosity of natural sediment mixtures is the grain size distribution (GSD). Therefore, a proper evaluation of the GSD is a prerequisite for explaining the spatial variations in porosity. For this purpose, the grain size distribution for each of the 55 sediment samples was determined (*Mineral density determination* section), taken to ascertain mineral density, using dry sieving on a 0.5 phi sieve set ranging from 0.063 to 125 mm. Each GSD was checked to ensure that the largest size clast did not constitute more than 5% of the total sample mass: 54 out of 55 GSDs complied with this rule and were considered representative. For each grain size distribution, the following parameters were determined as primary descriptors of the grain size distribution: geometric average grain size (D_g), median grain size (D_{50}), fraction content of grains smaller than 0.5 mm ($f_{<0.5}$), geometric standard deviation (σ_g), logarithmic standard deviation (σ_φ), geometric skewness (Sk_g) and logarithmic skewness (Sk_φ). Because calculation of σ_g, σ_φ, Sk_g and Sk_φ is not straightforward, the expressions that were used are included below:

$$D_g = \exp\left(\sum_i f_i \cdot \ln D_i\right) \qquad (6)$$

$$\sigma_g = \exp\left(\sqrt{\sum_i f_i \cdot \left(\ln\frac{D_i}{D_g}\right)^2}\right) \qquad (7)$$

$$Sk_g = \frac{\sum_i f_i \cdot \left(\ln\frac{D_i}{D_g}\right)^3}{\ln\sigma_g^3} \qquad (8)$$

$$\sigma_\varphi = \sqrt{\sum_i f_i \cdot \left(\varphi_i - \sum_i f_i\varphi_i\right)^2} \qquad (9)$$

$$Sk_\varphi = \frac{\sum_i f_i \cdot \left(\varphi_i - \sum f_i\varphi_i\right)^3}{\sigma_\varphi^3} \qquad (10)$$

Here f_i is the fraction content of sediment in size class i, D_i is the characteristic sediment diameter for size class i, expressed on the millimetre-scale, and φ_i is the characteristic sediment diameter for size class i, expressed on the φ-scale.

RESULTS

Validation of the nuclear density gauge

The three successive NDG measurements at each location show close agreement to one another. The standard deviation of the three successive water content measurements ranged between 0.0% and 0.4%, whereas the standard deviation of the three successive total wet density measurements ranged between 0.0 kg m^{-3} and 20 kg m^{-3}.

Comparison of porosity determined using the NDG to porosity of the prototype sediments (Table 2) indicates a good performance of NDG in direct transmission mode. The backscatter mode overestimated porosity values in both boxes, but this mode was not used for the NDG measurement in the field.

Comparison of porosity measured using the NDG to porosity measured using the water displacement method (Fig. 6A), shows a strong correlation between both porosity values. There is no sign of a systematic difference: the datapoints scatter around the line of perfect agreement with an RMSE of about 0.03. This is considered acceptable, because: (i) the measurement volume was not exactly the same for both methods; and (ii) it is impossible to reproduce the sediment packing as it existed in its original field condition in the laboratory.

Comparison of porosity determined with the NDG to porosity determined with the photogrammetry method (Fig. 6B), showed that both methods produced similar results with an RMSE of about 0.04. The difference can be attributed to the fact that the exact measurement volume is not the same for both methods. However, comparing the performance similarity of these methods with additional data would make the evaluation clearer.

Spatial variability of mineral density and porosity

The mineral density of the sediments in our study area varied between 2493 kg m^{-3} and 2730 kg m^{-3}. In order to compare mineral densities of different sedimentological environments, the Kruskal-Wallis test was conducted to determine if they come from the same population (or, equivalently, from different populations with the same distribution). It has been shown that, the mean mineral densities at the confluence site (2656 kg m^{-3}) and the bar site (2641 kg m^{-3}) were nearly similar, but significantly ($P < 0.05$ according to a Kruskal-Wallis test) higher than the mean mineral densities at the delta site

Table 2. Nuclear density gauge (NDG) accuracy assessment on sediment boxes: ρ_s, mineral density; V_s, solid fraction volume; V_t, total volume of a sediment sample; n_{true}, porosity of the prototype sediments; n_{NDG}, porosity measured using the NDG.

Box	Sediment (kg)	Water (l)	ρ_s (kg m^{-3})	V_s (l)	V_t (l)	n_{true} (–)	n_{NDG} (–) Backscatter	Direct transmission
1	66.6	0	2638	25.3	39.1	0.35	0.44	0.38
2	75.8	0	2609	29.1	38.7	0.25	0.32	0.25
2	75.8	2	2609	29.1	42.1	0.31	–	0.30
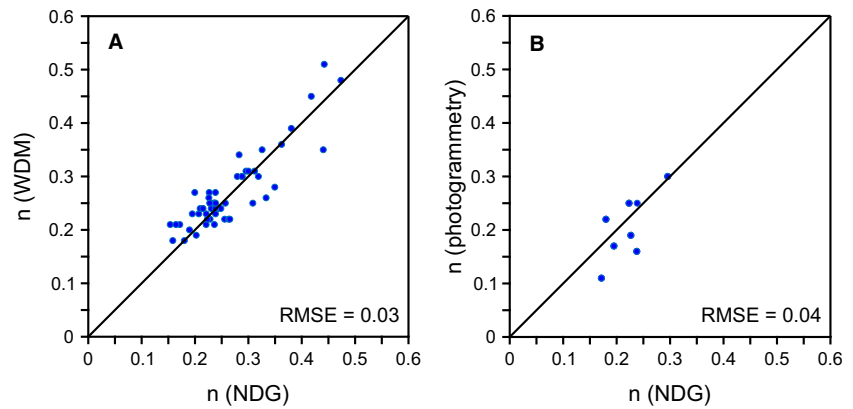
Fig. 6. Comparison of porosity (*n*) measured with nuclear density gauge (NDG) and (A) water displacement method (WDM), and (B) photogrammetry technique.

Table 3. Descriptive statistics of mineral density (ρ_s) at each measurement site.

Site	Number of measurements	ρ_s (kg m^{-3})	
		Mean	Standard deviation
Confluence	14	2656	40.7
Delta	5	2562	58.4
Bar	19	2641	34.6
Secondary channel	17	2571	36.4

(2562 kg m^{-3}) and the secondary channel site (2571 kg m^{-3}; Table 3).

In order to calculate the mean porosity, the outliers were first identified and excluded from the porosity dataset. As a result, one outlier was excluded from the confluence and another one from the bar site (*n* = 0.44; Fig. 5A and C). In this way, the mean porosity for the entire NDG porosity dataset was 0.25 (Table 4). Clear differences exist between the four different sedimentological environments, with significantly (*P* < 0.05) lower mean porosity values for the confluence (*n* = 0.23) and bar (*n* = 0.22) than for the delta (*n* = 0.31) and secondary channel (*n* = 0.29). For three of the environments, the standard deviation of porosity (Table 4) equalled 0.03; only the secondary channel showed a higher standard deviation of 0.08. The overall standard deviation of the NDG porosity dataset equalled 0.06. These values represent the first descriptor of the spatial variability presented in this study. The cross-sectional and longitudinal variations of porosity in the four sedimentological environments are shown in Figs 7 to 10.

The lagged scatter plots of porosity pairs (Fig. 11) show a significant correlation between measurements situated less than 3 m apart: the linear correlation coefficient is 0.534 for lagged distances between 0.0 m and 1.5 m, and is 0.559 for lagged distances between 1.5 m and 3.0 m. The correlations vanish after a few metres. The semi-variogram (Fig. 12A) shows the absence of any spatial correlation in porosity for distances greater than 4 m. However, Fig. 12B reveals a spatial dependence for distances of up to 4 m, which means that locations closer to one another have more similar porosity. The sill of the variogram is 0.0037, which is equal to the variance of the entire porosity dataset (the square of the standard deviation shown in Table 4).

Spatial variation of grain size

The differences between the four sedimentological environments with respect to grain size characteristics are shown in Table 5. The bar sediments (D_{50} = 11.78 mm) and the confluence sediments (D_{50} = 13.17 mm) were significantly (*P* < 0.05 according to a Kruskal-Wallis test) coarser than the delta sediments (D_{50} = 4.58 mm). They were also coarser than the secondary channel (D_{50} = 8.48 mm), although this difference is not statistically significant (*P* > 0.05). Furthermore, the latter two environments showed a relatively high proportion of fines ($f_{<0.5}$) compared to the bar and the confluence site (*P* < 0.05).

The secondary channel sediments had a significantly (*P* < 0.05) higher standard deviation than the bar and the confluence sediments. This site also had a higher standard deviation than the delta, although this difference is not

Table 4. Descriptive statistics of porosity (*n*) variation at each measurement site. Values include the entire data set of this study except two outliers located at the confluence and the bar site (*n* = 0.44).

Site	Number of measurements	n (–)				
		Minimum	Maximum	Mean	Median	Standard deviation
Confluence	47	0.15	0.31	0.23	0.23	0.03
Delta	18	0.28	0.36	0.31	0.30	0.03
Bar	18	0.16	0.26	0.22	0.22	0.03
Secondary channel	16	0.16	0.47	0.29	0.28	0.08
All samples	99	0.15	0.47	0.25	0.24	0.06

statistically significant ($P > 0.05$). Furthermore, the secondary channel includes more fine skewed samples than the other sites. These differences are statistically significant at $P < 0.05$.

The lagged scatter plots for grain size characteristics are summarized in Table 6, showing the absence of any spatial correlation for distances greater than 3 m (low *r*-value and high *P*-value). In some cases, a spatial correlation existed for distances of up to 3 m, however, the trend is not mostly statistically significant ($P > 0.05$). The cross-sectional and longitudinal variations of grain size characteristics for four different environments, shown in Figs 7 to 10, further confirm the absence of any spatial correlation.

The correlation between sediment characteristics and porosity

In an attempt to explain the spatial variation in porosity, the correlation between grain size characteristics and porosity was investigated. In Fig. 13, the relationships between grain size parameters (σ_φ, Sk_φ, and $f_{<0.5}$) and porosity were explored using the line of best fit (red dashed line). The line of best fit resulted from a linear regression analysis. In linear regression, the 'F-test' examines the significance of a fitted model i.e. the line of best fit.

Our study did not reveal any correlation between porosity and mean grain size (D_g) or median grain size (D_{50}). A weak, but significant, correlation (low *P*-values of the *F*-test) however existed between porosity and grain size parameters such as standard deviation (σ_g or σ_φ), skewness (Sk_g or Sk_φ) and the fraction content of grains smaller than 0.5 mm ($f_{<0.5}$). Porosity decreased with increasing standard deviation, increasing skewness of the GSD, and decreasing fine sediment fraction.

DISCUSSION

The suitability of nuclear density gauging for porosity measurements in rivers

Close agreement of the three successive nuclear density gauge (NDG) measurements at each location shows that NDG measurements are precise and repeatable. Furthermore, the strong correlation between porosity values measured using the NDG and porosity values measured using the water displacement and photogrammetry techniques, shows that they are accurate too. Therefore, NDG can be considered to be an appropriate technique for porosity measurements in rivers. Because NDG measurements are easy and quick, NDG is a good option for field studies in which many porosity measurements are required.

The use for NDG for porosity measurements, however, also has some limitations. Firstly, NDG does not work in submerged conditions, so its use is limited to situations when the river bed surface is accessible such as during low-flow periods. Secondly, NDG requires a close contact between the device's bottom and the sediment surface; therefore, NDG can only be applied to even sediment surfaces, such as the subsurface sediments investigated in this study. If information is needed about the porosity of armour layers, which are notoriously uneven, the photogrammetry method described in Tabesh *et al.* (2019) is recommended.

Explaining the spatial variation in porosity

The semi-variogram analysis showed a spatial dependence of porosity for distances of up to 4 m, meaning that locations closer to each other have more similar porosity. It is expected that
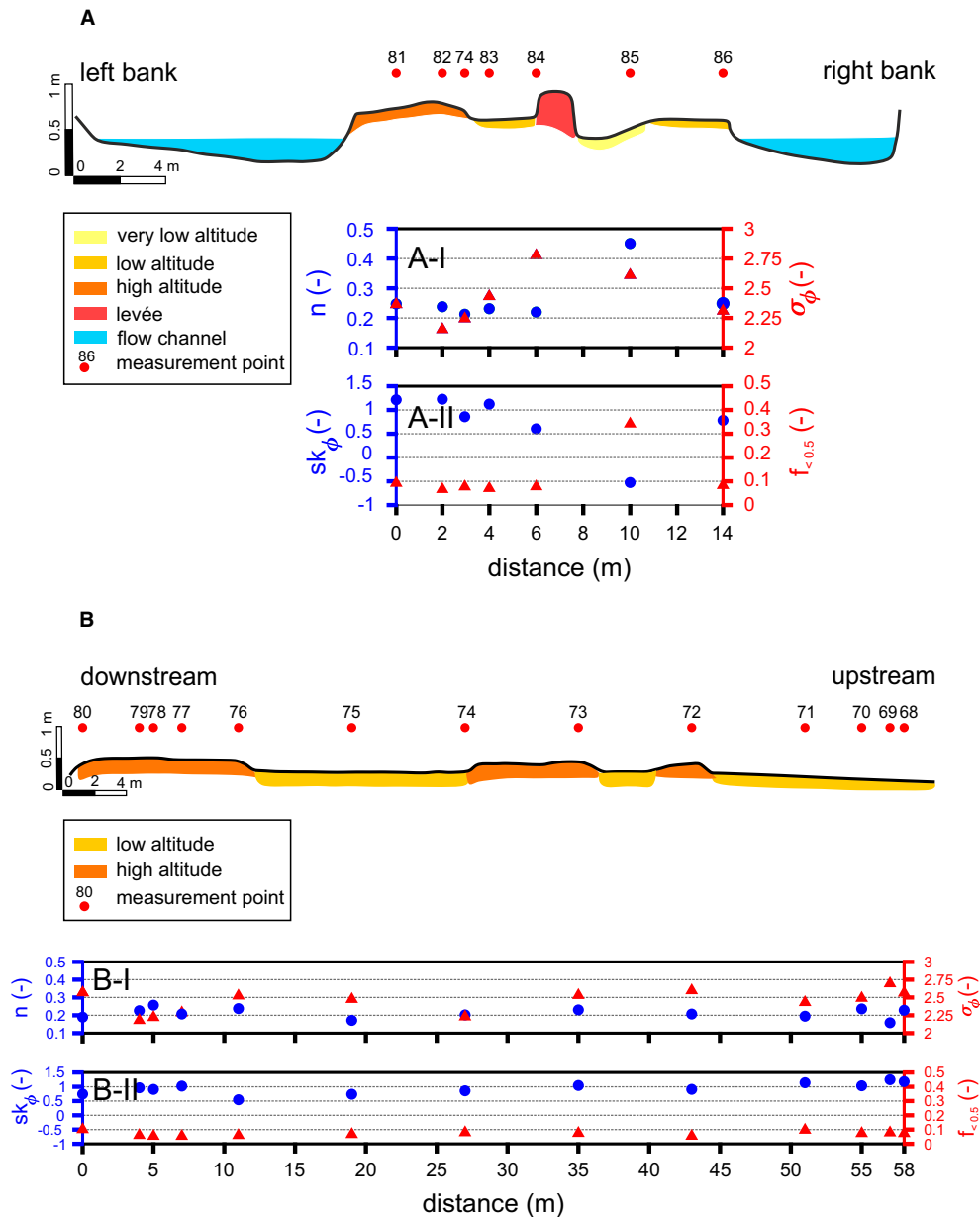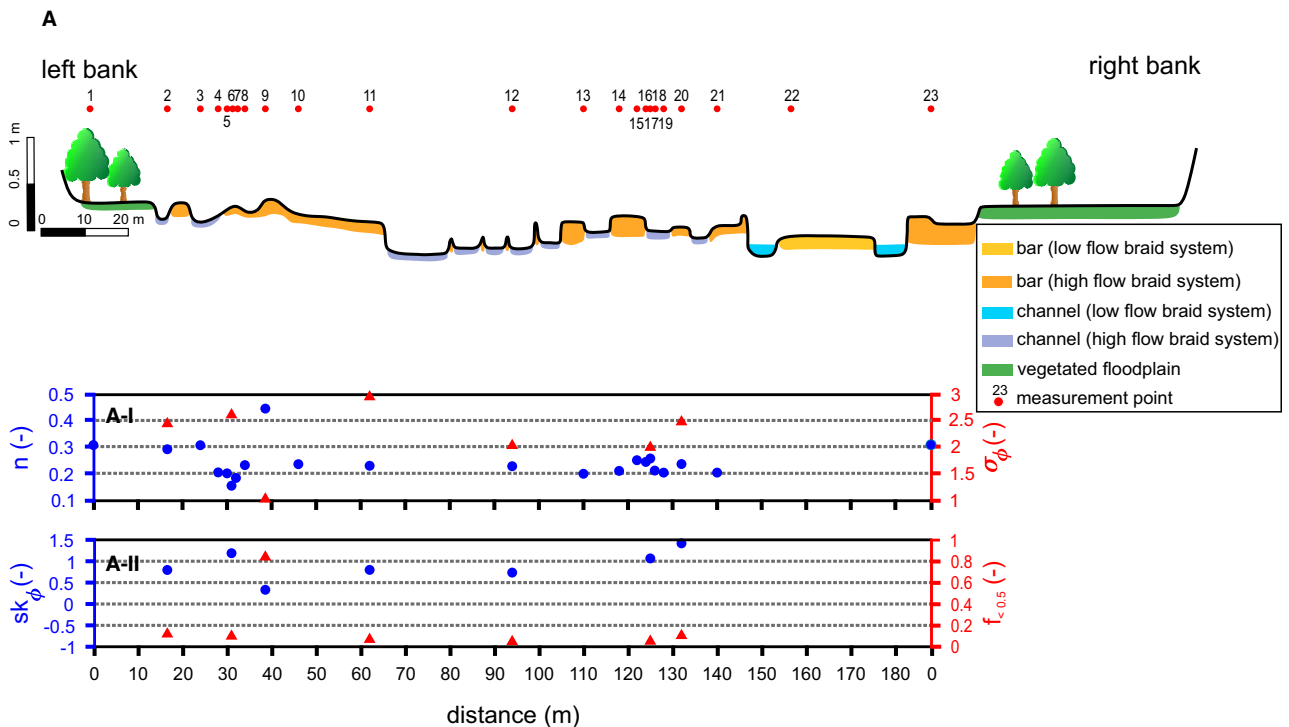
Fig. 7. (A) Schematic cross-sectional profile, (B) longitudinal profile at the bar site. (I) shows the variation of porosity (*n*) in the left vertical axis and logarithmic standard deviation (σ_φ) in the right vertical axis. (II) shows the variation of logarithmic skewness (Sk_φ) in the left vertical axis and fraction of fine grains smaller than 0.5 mm ($f_{<0.5}$) in the right vertical axis. The bar elevation is given relative to the local water level.

the spatial dependency of porosity is attributed to the small-scale patchiness phenomena. The presence of patches can be caused by some local sedimentological properties such as stone clusters and bedforms.

In most gravel-bed rivers, the sediment mixtures are often sorted into areas of similar grain size, producing discrete patches (Buffington & Montgomery, 1999; Yarnell *et al.*, 2006; Nelson

et al., 2010). On the North Fork Toutle River, Seal & Paola (1995) found that patch diameters range from less than 1 m to about 10 m. Moreover, Paola & Seal (1995) suggested that the patchiness would tend to arise in well-developed braiding morphologies with a poorly sorted, bimodal sediment distribution. Such a mechanism is likely in the studied braided river, in which poorly sorted ($\overline{\sigma}_\varphi = 2.6$), bimodal

Fig. 8. (A) Schematic cross-sectional profile at the confluence site. (I) shows the variation of porosity (*n*) in the left vertical axis and logarithmic standard deviation (σ_φ) in the right vertical axis. (II) shows the variation of logarithmic skewness (Sk_φ) in the left vertical axis and fraction of fine grains smaller than 0.5 mm ($f_{<0.5}$) in the right vertical axis.

sediment distributions were frequently observed. Therefore, in this study area, it was possible that the presence of patches (with a length scale of about 4 m) with similar sedimentological packing resulted in similar porosity.

Furthermore, the spatial dependency of porosity (with the length scale of 4 m) might be attributed to the presence of patches which are caused by bedforms. Fluvial deposits encompass a set of bedforms: (i) dunes and ripples which usually organize into bars; and (ii) bedload sheets which lie within channels (Bridge, 1993; Lunt *et al.*, 2004; Gibling, 2006). On the Saga-vanirktok River in northern Alaska, Lunt *et al.* (2004) showed that braid bars of a similar size to the one examined in this study were covered with a variety of surface depositional features, dunes and bedload sheets, that extended for distances in the same order of magnitude as the length scale of 4 m. On the Calamus River, Nebraska, Bridge *et al.* (1986) observed that most of the channel bed was covered with dunes with the lengths of 2 to 7 m at high flow stages and 1 to 4 m at low flow stages. Over these distances,

the bed configurations were quite homogenous. Therefore, similar sedimentological packing, and as a result similar porosity, might be expected.

In order to explain the spatial variation in porosity, the relationship between porosity and grain size characteristics as one of the major porosity controlling factors, has been assessed. In previous studies, the effect of the grain size characteristics on porosity has been quantified in some detail. For instance, Frings *et al.* (2011a) found that the median grain size (D_{50}) is unable to reproduce the observed variation in porosity, which was confirmed with the high *P*-values ($P > 0.05$) shown in Table 6. They also showed that porosity decreases with increasing standard deviation of grain size distribution, with bimodal particle mixtures generally having a lower porosity than unimodal mixtures. Our result confirmed these findings and also showed that with very poorly sorted sediments (high σ_φ), GSDs with the similar σ_φ values might result in various porosity values (Fig. 13A).

In this study, the effect of skewness of grain size distribution on porosity, which has not
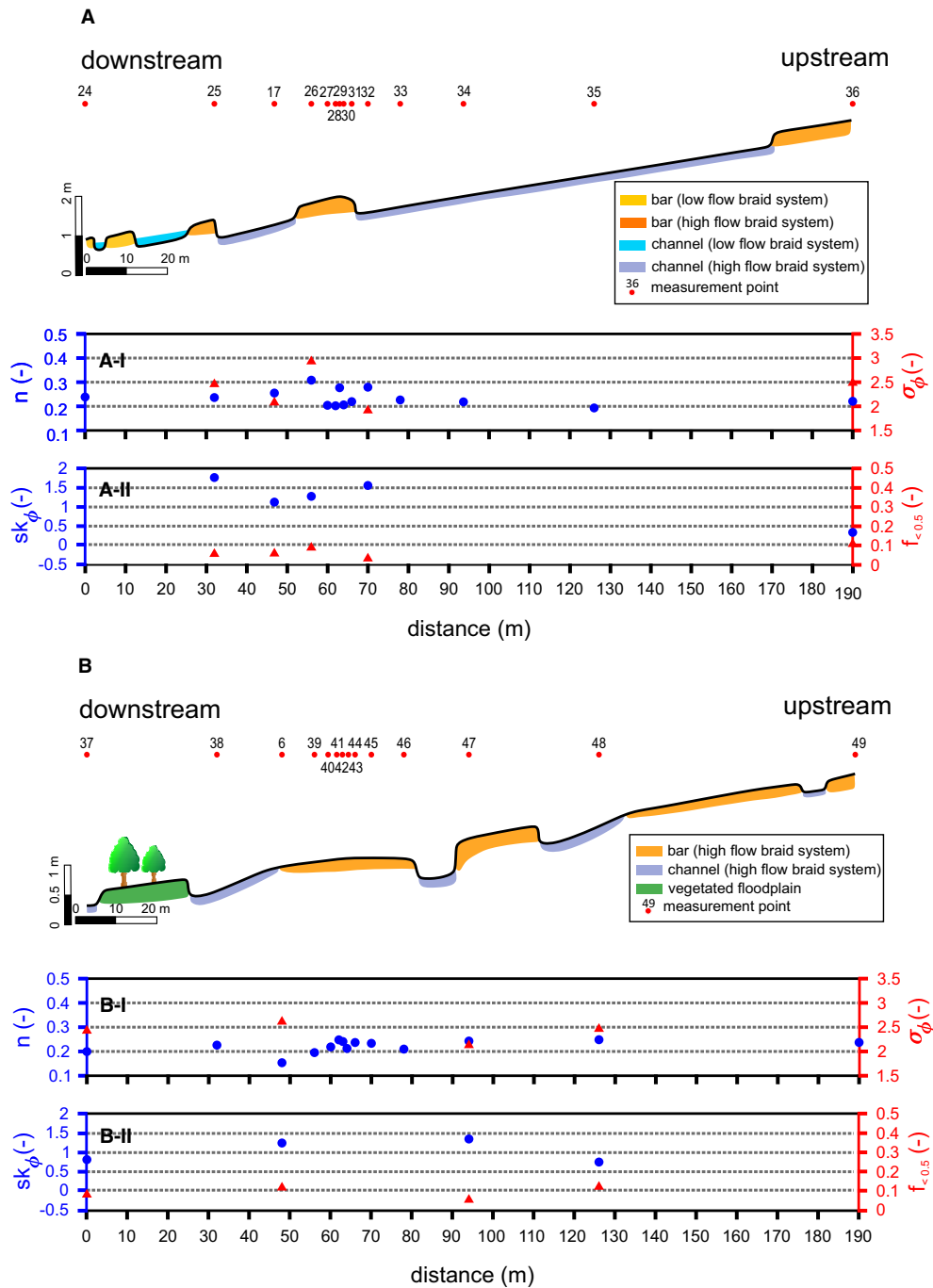
Fig. 9. (A) and (B) Schematic longitudinal profiles at the confluence site. (I) shows the variation of porosity (*n*) in the left vertical axis and logarithmic standard deviation (σ_φ) in the right vertical axis. (II) shows the variation of logarithmic skewness (Sk_φ) in the left vertical axis and fraction of fine grains smaller than 0.5 mm ($f_{<0.5}$) in the right vertical axis. Average gradient 0.016 (16 m km^{-1}).

been discovered or reported in previous studies, has been presented. Figure 13B shows that a GSD with coarse skewed shape (indicating a tail of coarser particles) is more likely to have lower porosity than with fine skewed shape (indicating an excess of fines). This is in good agreement with our results (Fig. 13B) presenting the effect of skewness of grain size distribution on porosity, which has not been discovered or reported in previous studies.
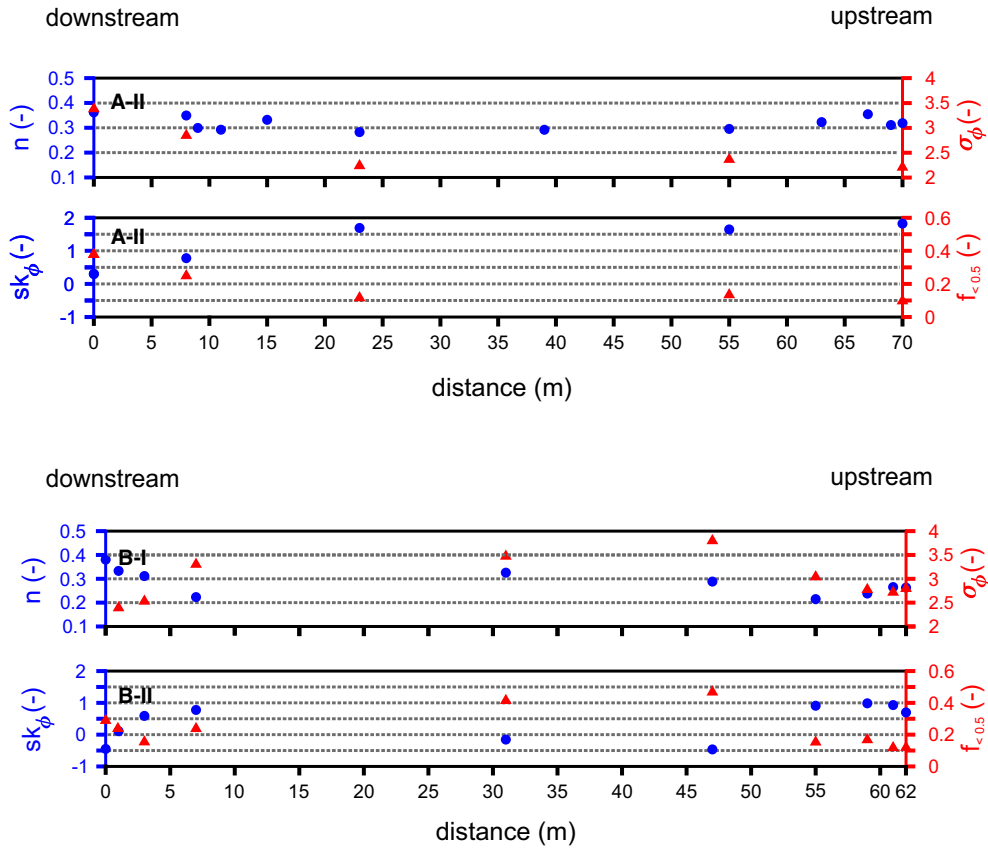
Fig. 10. (A) Schematic longitudinal profile at the delta site, (B) longitudinal profile at the secondary channel site. (I) shows the variation of porosity (*n*) in the left vertical axis and logarithmic standard deviation (σ_φ) in the right vertical axis. (II) shows the variation of logarithmic skewness (Sk_φ) in the left vertical axis and fraction of fine grains smaller than 0.5 mm ($f_{<0.5}$) in the right vertical axis.
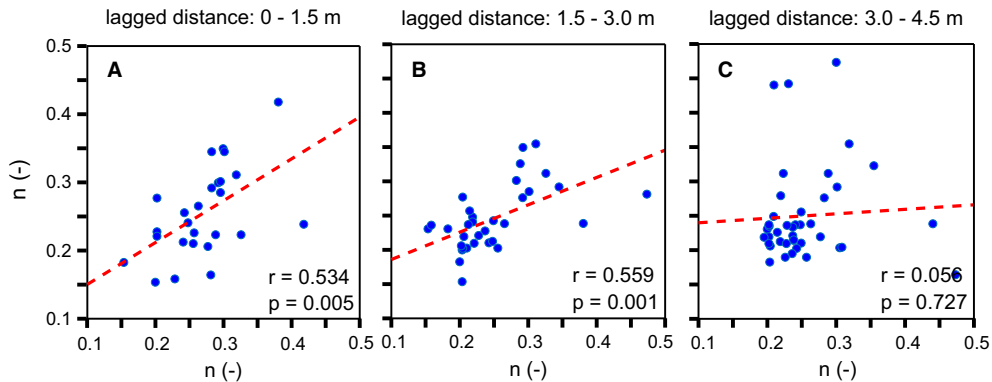

Fig. 11. Lagged scatter plots of pairs of porosity (*n*) grouped in three different lagged distances: (A) 0–1.5 m, (B) 1.5–3.0 m, (C) 3.0–4.5 m; r-value is the Pearson correlation coefficient, *P*-value is the significant level in the case of *P* < 0.05. Red dashed line represents the best fit line.

Fractional-packing models based on bimodal sediment mixtures (Koltermann & Gorelick, 1995; Kamann *et al.*, 2007) have suggested that porosity can be much better predicted by knowing the volume fraction of fine grains. As the volume fraction of fine grains increases within a
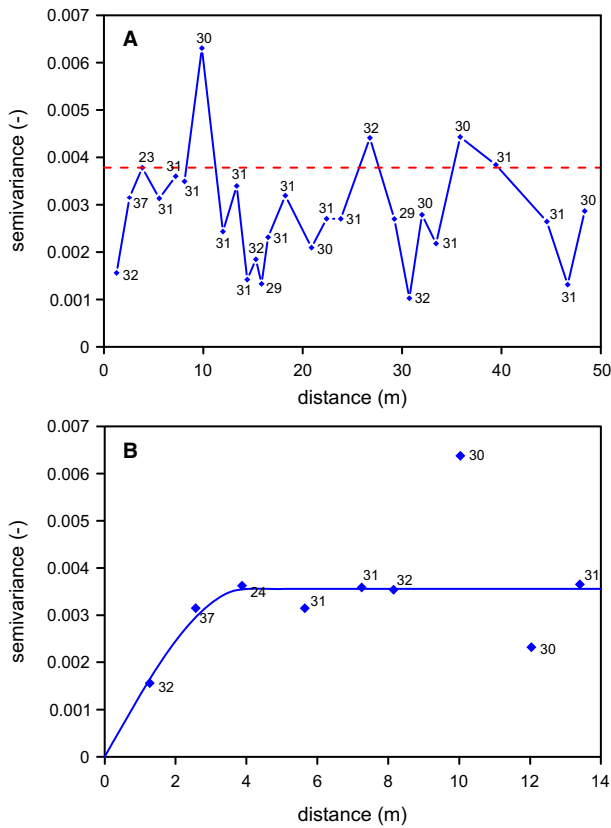
Fig. 12. Semi-variogram for the entire nuclear density gauge (NDG) porosity dataset across (A) 50 m, (B) 14 m of the measurement site. The number of pairs in each bin is written next to each point. The horizontal dashed line indicates the overall sample variance. Blue line represents the spherical model fitted to the sample variogram.

sediment mixture, the packing of the mixture changes which causes changes in porosity. Furthermore, Frings *et al.* (2011a) indicated that as

the content of fine grains smaller than 0.5 mm increases, porosity increases due to increasing importance of adhesion effects. Due to the adhesion effects, the surface of grains is covered with a thin layer of water and thus it separates the grains a little, resulting in increasing porosity. This finding has a good agreement with our results shown in Fig. 13C.

Although grain size characteristics (σ_φ, Sk_φ, and $f_{<0.5}$) have significant impact on porosity, the relationships between these parameters and porosity are not very strong (Fig. 13). Theoretically, porosity of sand–gravel mixtures must depend on grain size characteristics, and thus they should be able to explain porosity variations. However, this relationship is not sufficiently accounted for by the grain size parameters used in this study. This shows that in order to improve the explanation of porosity variations, other grain size characteristics or other porosity controlling parameters, such as grain shape or depositional conditions (Frings *et al.*, 2011b), need to be considered.

Guidelines for number of porosity samples

The analysis presented in this paper indicated that porosity point measurements are correlated over a distance of 4 m, but not beyond. Therefore, thousands of direct measurements are required to ensure an accurate characterization of the field site at this scale. This means that accurate characterization would be practically impossible or very difficult to achieve. Hence, a certain number of samples can be taken to have a reliable insight about the mean and variance of porosity. In fact, a limited number of sampling points allows an approximate

Table 5. Mean and standard deviation (STD) of the measured grain size characteristics (on a millimetre-scale and phi-scale) for all four sites: D_{50}, median grain size; D_g, geometric average grain size; σ_g, geometric standard deviation; σ_φ, logarithmic standard deviation; Sk_g, geometric skewness; Sk_φ, logarithmic skewness; $f_{<0.5}$ fine grains smaller than 0.5 mm.

Site	Number	D_{50} (mm)		D_g (mm)		σ_g (–)		σ_φ (-)		Sk_φ (–)*		$f_{<0.5}$ (–)	
		Mean	STD	Mean	STD	Mean	STD	Mean	STD	Mean	STD	Mean	STD
Confluence	14	13.17	6.81	8.57	4.63	5.33	1.52	2.35	0.47	0.98	0.41	0.14	0.21
Delta	5	4.58	1.72	2.98	1.50	6.57	2.51	2.64	0.50	1.25	0.67	0.19	0.12
Bar	19	11.78	3.97	7.78	2.36	5.58	0.69	2.47	0.18	0.88	0.40	0.10	0.06
Secondary channel	16	8.48	7.57	5.01	3.53	8.09	3.48	2.84	0.77	0.37	0.61	0.30	0.24
All samples	54	10.50	6.34	6.72	3.79	6.35	2.46	2.57	0.54	0.79	0.54	0.18	0.19

* $Sk_g = -Sk_\varphi$.

Table 6. Pair points of median grain size (D_{50}), logarithmic standard deviation (σ_{φ}), skewness (Sk_{φ}) and fine grains ($f_{<0.5}$) grouped in three different lagged distances: (left) 0–1.5 m, (middle) 1.5–3.0 m, (right) 3.0–4.5 m; *r*-value is the Pearson correlation coefficient, *P*-value is the significant level. Bold values denote statistical significance at the $P < 0.05$ level.

| Grain size characteristics	Lagged distance: 0–1.5 m		Lagged distance: 1.5–3.0 m		Lagged distance: 3.0–4.5 m	
	r-value	*P*-value	*r*-value	*P*-value	*r*-value	*P*-value
D_{50}	0.554	0.122	0.519	0.102	0.122	0.619
σ_{φ}	0.437	0.240	0.618	**0.043**	-0.388	0.101
Sk_{φ}	0.726	**0.027**	0.681	**0.021**	0.250	0.303
$f_{<0.5}$	0.329	0.387	0.676	**0.023**	0.251	0.300
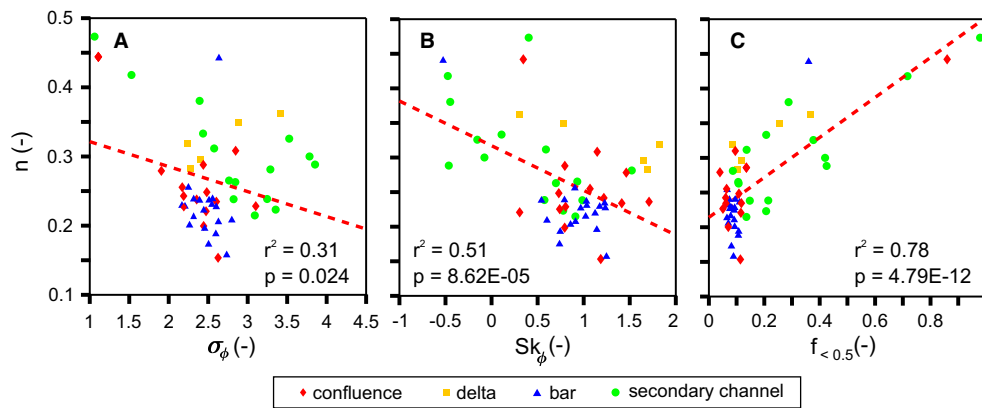
Fig. 13. The relation between: (A) logarithmic standard deviation of grain size distribution (GSD) (σ_{φ}); (B) logarithmic skewness of the GSD (Sk_{φ}); and (C) fraction of fine grains smaller than 0.5 mm ($f_{<0.5}$) and porosity (*n*) at four different sites. *P*-values are derived using the F-test and give significant differences in the case of $P < 0.05$. r^2-values determine the percentage of the data that is closest to the best fit line. Red dashed line represents the best fit line.

characterization of a field site. Furthermore, a good estimate of the mean porosity value can be used to convert measured volumetric changes of a river bed into sediment transport rates, which has been utilized in sediment budget analysis (Frings *et al.*, 2014). Church & Ferguson (2015) also showed that sediment transport rates can be trackable from morphological changes in a river, for which considering a reliable mean porosity is a prerequisite.

In order to obtain a good estimate of the mean porosity with a desired accuracy, a certain number of porosity measurements needs to be carried out. In this study, in order to assess the effect of the sampling number on the accuracy of a mean porosity, the porosity dataset at each site was randomly subsampled. Since the total number of NDG porosity samples at each

site was limited to 48, 18, 19 and 16 in confluence, delta, bar and secondary channel, respectively, the procedure of subsampling was conducted by replacement. To do so, during the procedure of subsampling at each site, between 1 and 50 samples of the total number of porosity samples were chosen. A subsample was generated from the uniformly distributed random integers (index between 1 and the total number of porosity samples at each site). Afterwards, porosity values corresponding to these random indices were selected. Then the mean and the standard deviation of porosity values of each subsample were calculated. Consequently, the accuracy of the mean porosity in each subsample was evaluated by calculating the standard error (*SE*) using the following expression:
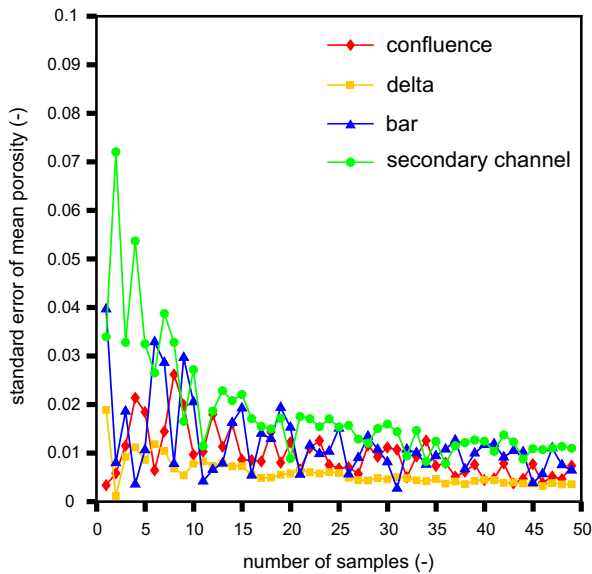
Fig. 14. The effect of sampling number on the standard error (*SE*) of the mean porosity at four different sites.

$$SE = \frac{\sigma}{\sqrt{\hat{N}}} \qquad (11)$$

where σ and $\hat{N}$ are the standard deviation of porosity values and number of porosity samples in one subsample, respectively. Figure 14 shows the decreasing of the standard error with increasing sample numbers at all four sites.

It has become clear that the required number of porosity samples to achieve a reliable mean porosity value strongly depends on the porosity spatial variability in an environment and the desired level of accuracy. Therefore, guidelines for the number of porosity samples (N) can be easily generated using Eq. 11. The first step to select a sufficient number of porosity samples can be done by setting *SE* to some predefined low accuracy level (for example 0.03). With the knowledge of porosity standard deviation (σ) in an environment, one can determine the number of porosity samples that is required to obtain the mean porosity with the desired level of accuracy.

In this study, the secondary channel site with the highest variation of grain size characteristics showed the highest variation of porosity, with a standard deviation of 0.08. This value can be considered as a safe, first recommendation of porosity standard deviation for situations without any prior knowledge about the standard deviation of porosity. Therefore, using Eq. 11, eight porosity samples appear to be required to obtain a mean porosity with an uncertainty of ±0.03 in an unknown environment. Generally, aiming at uncertainty below 0.03 gives an abrupt increase in sampling effort (for estimates with an uncertainty of 0.02 at least 16 samples are required), which might not be feasible in most river management studies.

All recommendations for the number of porosity samples given above refer to situations without any prior knowledge of the porosity variations with assumed porosity standard deviation of 0.08. However, if such *a priori* knowledge does exist and shows higher variability of porosity, considerably more porosity measurements are required (for example: about 12 samples if $\sigma = 0.1$).

CONCLUSIONS

This study provided a unique dataset of spatial variability in sediment porosity in sand–gravel bed rivers, which is valuable for researchers and river managers. The main conclusions of this study are:

1 Nuclear density gauging (NDG) is a time-saving and labour-saving technique that allows for an easy and quick measurement of sediment porosity in the field. It produces accurate porosity values with an RMSE of 0.03. This technique requires independent, accompanying measurement of mineral density and water content.
2 The four sedimentological environments in braiding rivers that were investigated in this study show different porosity, with mean porosity being significantly lower for the confluence and the bar than for the delta and secondary channel. The standard deviation of porosity equalled 0.08 for the secondary channel and 0.03 for the other three environments. This shows that spatial porosity variability is noticeable and cannot be neglected.
3 Spatial correlation in porosity values is present up to a distance of 4 m. For distances beyond 4 m, the porosity values are spatially uncorrelated. Consequently, it is not possible to estimate porosity by spatial extrapolation from points with known porosity, unless the extrapolation distance is less than 4 m.
4 The number of porosity samples required to obtain a reliable mean porosity value depends

on the spatial variation of porosity and the desired level of accuracy. At least eight measurements of porosity are required to obtain a reliable estimate of the mean porosity in a sedimentary environment, i.e. with uncertainty <0.03.

5 Although grain size characteristics (σ_φ, Sk_φ, and $f_{<0.5}$) have significant impact on porosity, the relationships between these parameters and porosity are not very strong. This shows that in order to explain porosity variations, other porosity controlling parameters need to be considered.

ACKNOWLEDGEMENTS

DATA AVAILABILITY STATEMENT

The data that supports the findings of this study are available in the supplementary material of this article.

NOMENCLATURE

V_s	Solid fraction volume, m^3
V_t	Total sediment volume (including pores), m^3
n	Porosity, dimensionless
n_{NDG}	Porosity measured using nuclear density gauge, dimensionless
n_{true}	Porosity of the prototype sediments, dimensionless
ρ_t	Total wet density, kg m^{-3}
ρ_s	Mineral density, kg m^{-3}
η	Water content (mass ratio of water and dry sediment), %
η_{NDG}	Water content measured using nuclear density gauge, %
η_{lab}	Oven-dried water content, %
h	Lag distance, m
γ	Semi-variance, dimensionless
$n(x_i)$	Porosity measured at location x_i, dimensionless
N	Number of porosity pair points separated by lag h, dimensionless
D_{10}	10th percentile of the grain size distribution, m
D_{50}	Median grain size, m
D_{90}	90th percentile of the grain size distribution, m
D_i	Characteristic sediment diameter for size class i, m
D_g	Geometrically averaged grain size, m
σ_g	Geometric standard deviation of the grain size distribution, dimensionless
σ_φ	Logarithmic standard deviation of the grain size distribution (φ scale), dimensionless
$\overline{\sigma}_\varphi$	Averaged logarithmic standard deviation of the grain size distribution (φ scale), dimensionless
Sk_g	Geometric skewness of the grain size distribution, dimensionless
Sk_φ	Logarithmic skewness of the grain size distribution (φ scale), dimensionless
φ_i	Characteristic sediment diameter for size class i (φ scale), dimensionless
f_i	Fraction content of sediment in size class i, dimensionless
$f_{<0.5}$	Fraction content of grains smaller than 0.5 mm, dimensionless
SE	Standard error of mean porosity, dimensionless
σ	Standard deviation of porosity values in one subsample, dimensionless
$\hat{N}$	Number of porosity samples in one subsample, dimensionless

REFERENCES

Abderrezzak, K.E.K., **Moran, A.D.**, **Tassi, P.**, **Ata, R.** and **Hervouet, J.-M.** (2016) Modelling river bank erosion using a 2D depth-averaged numerical model of flow and non-cohesive, non-uniform sediment transport. *Adv. Water Resour.*, **93**, 75–88.

Argent, D.G. and **Flebbe, P.A.** (1999) Fine sediment effects on brook trout eggs in laboratory streams. *Fish. Res.*, **39**, 253–262.

Athy, L.F. (1930) Density, porosity, and compaction of sedimentary rocks. *Am. Assoc. Pet. Geol. Bull.*, **14**, 1–22.

Bear, J. (1972) *Dynamics of Fluids in Porous Media.* Elsevier, New York.

Blom, A. (2003) *A Vertical Sorting Model for Rivers with Non-uniform Sediment and Dunes.* University of Twente, Enschede.

Boulton, A.J., **Findlay, S.**, **Marmonier, P.**, **Stanley, E.H.** and **Valett, H.M.** (1998) The functional significance of the hyporheic zone in streams and rivers. *Annu. Rev. Ecol. Syst.*, **29**, 59–81.

Bridge, J.S. (1993) The interaction between channel geometry, water flow, sediment transport and deposition in braided rivers. *Geol. Soc. London Spec. Publ.*, **75**(1), 13–71.

Bridge, J.S., **Smith, N.D.**, **Trent, F.**, **Gabel, S.L.** and **Bernstein, P.** (1986) Sedimentology and morphology of a low sinuosity river: Calamus River, Nebraska Sand Hills. *Sedimentology*, **33**(6), 851–870.

Buffington, J.M. and **Montgomery, D.R.** (1999) A procedure for classifying textural facies in gravel-bed rivers. *Water Resour. Res.*, **35**, 1903–1914.

Bui, V., **Bui, M.** and **Rutschmann, P.** (2019) Advanced numerical modeling of sediment transport in gravel-bed rivers. *Water*, **11**, 550.

Carling, P.A. and **Reader, N.A.** (1982) Structure, composition and bulk properties of upland stream gravels. *Earth Surf. Process. Land.*, **7**, 349–365.

Christakos, G. (1992) *Random Field Models in Earth Sciences.* Academic Press, San Diego.

Church, M. and **Ferguson, R.I.** (2015) Morphodynamics: rivers beyond steady state. *Water Resour. Res.*, **51**, 1883–1897.

Church, M., **Wolcott, J.F.** and **Fletcher, W.K.** (1991) A test of equal mobility in fluvial sediment transport: behavior of the sand fraction. *Water Resour. Res.*, **27**, 2941–2951.

Chwang, A.T. and **Chan, A.T.** (1998) Interaction between porous media and wave motion. *Annu. Rev. Fluid Mech.*, **30**, 53–84.

Clayton, J.A. and **Pitlick, J.** (2007) Spatial and temporal variations in bed load transport intensity in a gravel bed river bend. *Water Resour. Res.*, **43**, W02426.

Cressie, N. (1985) Fitting variogram models by weighted least squares. *J. Int. Assoc. Math. Geol.*, **17**, 563–586.

Cressie, N. and **Hawkins, D.M.** (1980) Robust estimation of the variogram: I. *J. Int. Assoc. Math. Geol.*, **12**, 115–125.

Cui, Y. (2007) The unified gravel-sand (TUGS) model: Simulating sediment transport and gravel/sand grain size distributions in gravel-bedded rivers. *Water Resour. Res.*, **43**, W10436.

Desmond, K.W. and **Weeks, E.R.** (2014) Influence of particle size distribution on random close packing of spheres. *Phys. Rev. E*, **90**, 022204.

Deutsch, C.V. and **Journel, A.G.** (1992) *Geostatistical Software Library and User's Guide.* Oxford University Press, New York, 340 pp.

Domenico, P.A. and **Schwartz, F.W.** (1998) *Physical and Chemical Hydrogeology.* Wiley, New York, 506 pp.

Esteves, M., **Legout, C.**, **Navratil, O.** and **Evrard, O.** (2019) Medium term high frequency observation of discharges and suspended sediment in a Mediterranean mountainous catchment. *J. Hydrol.*, **568**, 562–574.

Frings, R.M. (2011) Sedimentary characteristics of the gravel-sand transition in the River Rhine. *J. Sediment. Res.*, **81**, 52–63.

Frings, R.M., **Gehres, N.**, **Promny, M.**, **Middelkoop, H.**, **Schüttrumpf, H.** and **Vollmer, S.** (2014) Today's sediment budget of the Rhine River channel, focusing on the Upper Rhine Graben and Rhenish Massif. *Geomorphology*, **204**, 573–587.

Frings, R.M., **Kirsch, F.** and **Schüttrumpf, H.** (2012) The transition between gravel-bed rivers and sand-bed rivers. In: *River Flow 2012* (Ed. Murillo Munos, R.E.), pp. 629–634. Taylor and Francis, London.

Frings, R.M., **Kleinhans, M.G.** and **Vollmer, S.** (2008) Discriminating between pore-filling load and bed-structure load: a new porosity-based method, exemplified for the river Rhine. *Sedimentology*, **55**, 1571–1593.

Frings, R.M., **Ottevanger, W.** and **Sloff, K.** (2011a) Downstream fining processes in sandy lowland rivers. *J. Hydraul. Res.*, **49**, 178–193.

Frings, R.M., **Schüttrumpf, H.** and **Vollmer, S.** (2011b) Verification of porosity predictors for fluvial sand-gravel deposits. *Water Resour. Res.*, **47**, W07525.

Gibling, M.R. (2006) Width and thickness of fluvial channel bodies and valley fills in the geological record: a literature compilation and classification. *J. Sediment. Res.*, **76**, 731–770.

Goff, J.A., **Wheatcroft, R.A.**, **Lee, H.**, **Drake, D.E.**, **Swift, D.J.P.** and **Fan, S.** (2002) Spatial variability of shelf sediments in the STRATAFORM natural laboratory, Northern California. *Cont. Shelf Res.*, **22**, 1199–1223.

Gringarten, E. and **Deutsch, C.V.** (2001) Teacher's aide variogram interpretation and modeling. *Math. Geol.*, **33**, 507–534.

Hassan, M.A., **Egozi, R.** and **Parker, G.** (2006) Experiments on the effect of hydrograph characteristics on vertical grain sorting in gravel bed rivers. *Water Resour. Res.*, **42**, W09408.

Hatch, C.E., **Fisher, A.T.**, **Ruehl, C.R.** and **Stemler, G.** (2010) Spatial and temporal variations in streambed hydraulic conductivity quantified with time-series thermal methods. *J. Hydrol.*, **389**, 276–288.

Kamann, P.J., **Ritzi, R.W.**, **Dominic, D.F.** and **Conrad, C.M.** (2007) Porosity and permeability in sediment mixtures. *Ground Water*, **45**, 429–438.

Kleinhans, M.G. (2001) The key role of fluvial dunes in transport and deposition of sand–gravel mixtures, a preliminary note. *Sediment. Geol.*, **143**, 7–13.

Kleinhans, M.G. (2005) Upstream sediment input effects on experimental dune trough scour in sediment mixtures. *J. Geophys. Res. Earth Surf.*, **110**, F04S06.

Kleinhans, M.G., **Wilbers, A.W.E.**, **De Swaaf, A.** and **Van Den Berg, J.H.** (2002) Sediment supply-limited bedforms in sand-gravel bed rivers. *J. Sediment. Res.*, **72**, 629–640.

Koltermann, C.E. and **Gorelick, S.M.** (1995) Fractional packing model for hydraulic conductivity derived from sediment mixtures. *Water Resour. Res.*, **31**, 3283–3297.

Lisle, T.E. and **Hilton, S.** (1999) Fine bed material in pools of natural gravel bed channels. *Water Resour. Res.*, **35**, 1291–1304.

Lunt, I.A., **Bridge, J.S.** and **Tye, R.S.** (2004) A quantitative, three-dimensional depositionl model of gravelly braided rivers. *Sedimentology*, **51**, 377–414.

Matheron, G. (1963) Principles of geostatistics. *Econ. Geol.*, **58**, 1246–1266.

Miwa, H. and **Parker, G.** (2017) Effects of sand content on initial gravel motion in gravel-bed rivers. *Earth Surf. Process. Landforms*, **42**, 1355–1364.

Morin, R.H. (2006) Negative correlation between porosity and hydraulic conductivity in sand-and-gravel aquifers at Cape Cod, Massachusetts, USA. *J. Hydrol.*, **316**, 43–52.

Mulatu, C., **Crosato, A.**, **Moges, M.**, **Langendoen, E.** and **McClain, M.** (2018) Morphodynamic trends of the Ribb River, Ethiopia, prior to dam construction. *Geosciences*, **8**, 255.

Navratil, O., **Evrard, O.**, **Esteves, M.**, **Legout, C.**, **Ayrault, S.**, **Némery, J.**, **Mate-Marin, A.**, **Ahmadi, M.**, **Lefèvre, I.**, **Poirel, A.** and **Bonté, P.** (2012) Temporal variability of suspended sediment sources in an alpine catchment combining river/rainfall monitoring and sediment fingerprinting. *Earth Surf. Process. Landforms*, **37**, 828–846.

Navratil, O., **Legout, C.**, **Gateuille, D.**, **Esteves, M.** and **Liebault, F.** (2010) Assessment of intermediate fine sediment storage in a braided river reach (southern French Prealps). *Hydrol. Process.*, **24**, 1318–1332.

Nelson, P.A., **Dietrich, W.E.** and **Venditti, J.G.** (2010) Bed topography and the development of forced bed surface patches. *J. Geophys. Res. Earth Surf.*, **115**, F04024.

Noack, M. (2012) *Modelling Approach for Interstitial Sediment Dynamics and Reproduction of Gravel-Spawning Fish*. Inst. für Wasser- und Umweltsystemmodellierung.

Paola, C. and **Seal, R.** (1995) Grain size patchiness as a cause of selective deposition and downstream fining. *Water Resour. Res.*, **31**, 1395–1407.

Pebesma, E.J. (2004) Multivariable geostatistics in S: the gstat package. *Comput. Geosci.*, **30**, 683–691.

Ramanathan, R., **Guin, A.**, **Ritzi, R.W.**, **Dominic, D.F.**, **Freedman, V.L.**, **Scheibe, T.D.** and **Lunt, I.A.** (2010) Simulating the heterogeneity in braided channel belt deposits: a geometric-based methodology and code. *Water Resour. Res.*, **46**, W04515.

Ryan, S.E., **Porth, L.S.** and **Troendle, C.A.** (2002) Defining phases of bedload transport using piecewise regression. *Earth Surf. Process. Landforms*, **27**, 971–990.

Sadeghiamirshahidi, M. and **Vitton, S.J.** (2019) Analysis of drying and saturating natural gypsum samples for mechanical testing. *J. Rock Mech. Geotech. Eng.*, **11**, 219–227.

Seal, R. and **Paola, C.** (1995) Observations of downstream fining on the North Fork Toutle River near Mount St. Helens, Washington. *Water Resour. Res.*, **31**, 1409–1419.

Seitz, L., **Haas, C.**, **Noack, M.** and **Wieprecht, S.** (2018) From picture to porosity of river bed material using Structure-from-Motion with Multi-View-Stereo. *Geomorphology*, **306**, 80–89.

Selby, M.J. (1993) *Hillslope Materials and Processes*, 2nd edn. Oxford University Press, Oxford.

Tabesh, M., **Hoffmann, T.**, **Vollmer, S.**, **Schüttrumpf, H.** and **Frings, R.M.** (2019) In-situ measurement of river-bed sediment porosity using Structure-from-Motion image analysis. *Geomorphology*, **338**, 61–67.

Ting, C.-L., **Lin, M.-C.** and **Cheng, C.-Y.** (2004) Porosity effects on non-breaking surface waves over permeable submerged breakwaters. *Coast. Eng.*, **50**, 213–224.

Vollmer, S. and **Kleinhans, M.G.** (2007) Predicting incipient motion, including the effect of turbulent pressure fluctuations in the bed. *Water Resour. Res.*, **43**, W05410.

Vollmer, S., **Ramos, F.S.**, **Daebel, H.** and **Kühn, G.** (2002) Micro scale exchange processes between surface and subsurface water. *J. Hydrol.*, **269**, 3–10.

Westoby, M.J., **Brasington, J.**, **Glasser, N.F.**, **Hambrey, M.J.** and **Reynolds, J.M.** (2012) "Structure-from-Motion" photogrammetry: a low-cost, effective tool for geoscience applications. *Geomorphology*, **179**, 300–314.

Wilcock, P.R. (1998) Two-fraction model of initial sediment motion in gravel-Bed rivers. *Science*, **280**, 410–412.

Wooster, J.K., **Dusterhoff, S.R.**, **Cui, Y.**, **Sklar, L.S.**, **Dietrich, W.E.** and **Malko, M.** (2008) Sediment supply and relative size distribution effects on fine sediment infiltration into immobile gravels. *Water Resour. Res.*, **44**, W03424.

Wu, W. and **Wang, S.S.Y.** (2006) Formulas for sediment porosity and settling velocity. *J. Hydraul. Eng.*, **132**, 858–862.

Yarnell, S.M., **Mount, J.F.** and **Larsen, E.W.** (2006) The influence of relative sediment supply on riverine habitat heterogeneity. *Geomorphology*, **80**, 310–324.

Zhang, Z.F., **Ward, A.L.** and **Keller, J.M.** (2011) Determining the porosity and saturated hydraulic conductivity of binary mixtures. *Vadose Zone J.*, **10** 313–321.

Supporting Information

Additional information may be found in the online version of this article:

Supinfo S1. This provides the dataset measured at four measurement sites. This dataset includes water content, porosity values measured with three different techniques and grain size parameters described in detail in the manuscript.